Remote Sensing Analysis of Ice Growth and Distribution in the Eastern Bering Sea

10

S. Lyn McNutt

NOAA
Pacific Marine Environmental Laboratory
Seattle, Washington

Present Affiliation:
Science Applications, Inc.
Bellevue, Washington

ABSTRACT

Ice thickness distribution and ice types for the eastern Bering Sea are inferred from satellite imagery and available aircraft data. These have been combined with analyses of ice bridging and floe trajectories to estimate movement and generation of ice within the pack. The location of the ice edge has been plotted for different dates using satellite imagery and ice analysis charts. The position of the edge and the variability of the geographic location of the ice types and thicknesses supports a theory of ice generation according to which ice forms along the leeward side of east-west-trending coasts, is advected to the south-southwest within the pack, is broken into floes near the ice edge by the effects of wave propagation, and melts at the edge when the thermodynamic limits of its stability are reached.

INTRODUCTION

In March, 1979, a joint experiment was conducted by NOAA, NASA, and the University of Washington in the Bering Sea. The NOAA ship *Surveyor*, stationed along the ice edge, provided ground truth for physical oceanographic and meteorological experiments (Pease 1979). Personnel from the University of Washington tracked floe movement at the ice edge and obtained core samples of the ice (Martin and Bauer, this volume). Researchers from Scott Polar Research Institute installed accelerometers on floes to assess wave propagation into the pack. The NASA C130 aircraft flew one mission 14 March 1979 over the *Surveyor*. The remote sensing equipment on board included a laser profilometer, a step-frequency radiometer (Harrington et al. 1979), a scatterometer, and a 23-cm format, 153.12-mm focal length camera. The NASA C131 aircraft flew over the same location a few hours later with a Side-looking Airborne Radar (SLAR) (Schertler 1979) on March 14. An additional track was flown in the Norton Sound area March 27. The *Surveyor* was in the ice during this period of maximum extent and at the beginning of a period of gradual retreat (Pease 1979).

This paper examines remote sensing evidence about the ice generation regime in the Bering Sea. Satellite imagery from the Defense Military Satellite Program, TIROS, and LANDSAT are used in conjunction with available ice charts from the Navy/NOAA Joint Ice Center (FWS) in Suitland, Maryland, and the above-mentioned field program, to formulate daily charts on ice conditions (Fig. 10-1). These charts were averaged to show weekly conditions. This data set is used to describe the ice regime in the eastern Bering Sea for March 1979.

Because ice in the Bering Sea is not a closed pack, as in the Arctic, the ice regime is qualitatively different. In the Bering Sea all ice is first-year ice and melts completely by the end of each season. The period 1-31 March 1979 was unique in that the ice was at maximum extent and also began a rapid, complete meltback to ice-free conditions.

WEEKLY AVERAGE ICE CONDITIONS

Four charts of weekly ice conditions have been produced by averaging daily charts. The charts cover the following periods: (1) March 1-7; (2) March 8-14; (3) March 15-21; (4) March 22-28. (Clouds obscured conditions at the very end of the month; extrapolations were not made.)

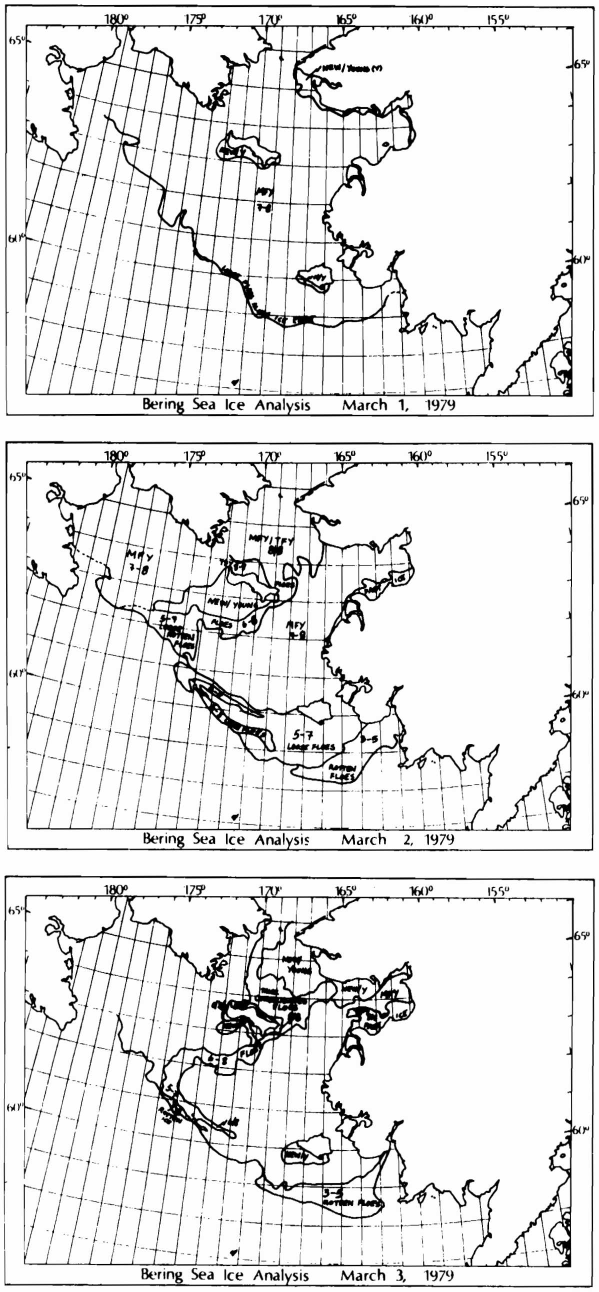

Figure 10-1. Daily charts on ice conditions in the Bering Sea. These analyses were compiled using Defense Military Satellite Program, TIROS, and LANDSAT imagery in comparison with FWS ice charts.

1. March 1-7 (Fig. 10-2). The ice is at maximum extent. Significant features include polynyas south of St. Lawrence Island and Nunivak Island and south of the western mainland in Norton Sound; floes which stream from the east of St. Lawrence Island to the south and southwest around the polynya area; the thick first-year ice (120 cm-2 m) north of St. Lawrence Island and Nunivak Island; and loose floes and streamers along the ice edge.

2. March 8-14 (Fig. 10-3). This week showed little change in ice conditions from the previous week; however, the ice continued to advance during the early part of the week and then began a gradual retreat.

3. March 15-21 (Fig. 10-4). A warming trend began during this week, accompanied by a reversal of northeast winds to a southerly direction (Pease, this volume). Breakup began and is especially noticeable in areas near the coast previously occupied by young first-year ice and polynyas.

4. March 22-28 (Fig. 10-5). This figure shows the effects of the breakup due to a warming trend. There is open water north of St. Lawrence Island and west of the mainland. The stream of floes around the south-southwest coast of St. Lawrence Island is still evident as are the floes and thicker ice west of the island.

The geographic constancy of features such as floe streamers, polynyas, and ice bands along the edge supports a theory of ice generation for the eastern Bering Sea like that which was proposed for the western Bering Sea by Loshchilov (1974) during the BESEX experiment. A schematic diagram (Fig. 10-6) shows that the ice, when at maximum extent, operates like a conveyor belt. The ice is formed in the leeward side of the east-west trending coasts and is advected downwind into the pack. This has also been observed by Muench and Ahlnäs (1976) and Ahlnäs and Wendler (1979). As the ice advances, it thickens and continues to be blown downwind to the edge, where it melts. This type of morphology for Bering Sea ice is evidenced by cores taken from the ice (Martin and Bauer, this volume, Martin and Kauffman 1979, Gloerson et al. 1974), which show ice compaction north of the islands and divergence around the islands and along the edge of the pack. The ice in the area to the east of St. Lawrence Island changes gradually from compaction to divergence. This is due, in part, to the shape of the ice pack, which is formed in a more constricted area than the one to which it is advected. Remote sensing data collected in March support the hypothesis that (1) ice is formed in the leeward side of east-west trending coasts under a dominant wind regime from the northeast; (2) ice is compacted north of the islands; (3) ice diverges around the islands; (4) ice at the seaward edge has reached its thermodynamic limit and is in the process of decay; and (5) ice retreat during breakup progresses most rapidly into the areas of thinner ice which had been supplying ice to the rest of the pack.

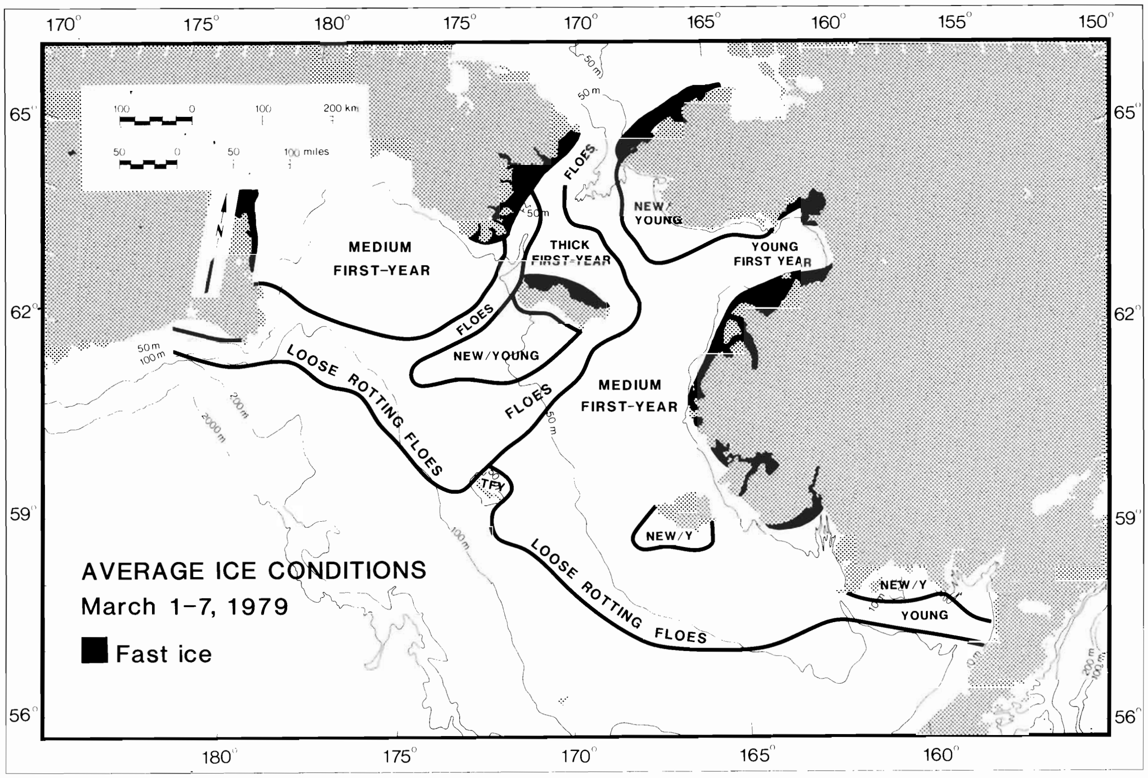

Figure 10-2. Weekly average ice conditions, 1-7 March 1979.

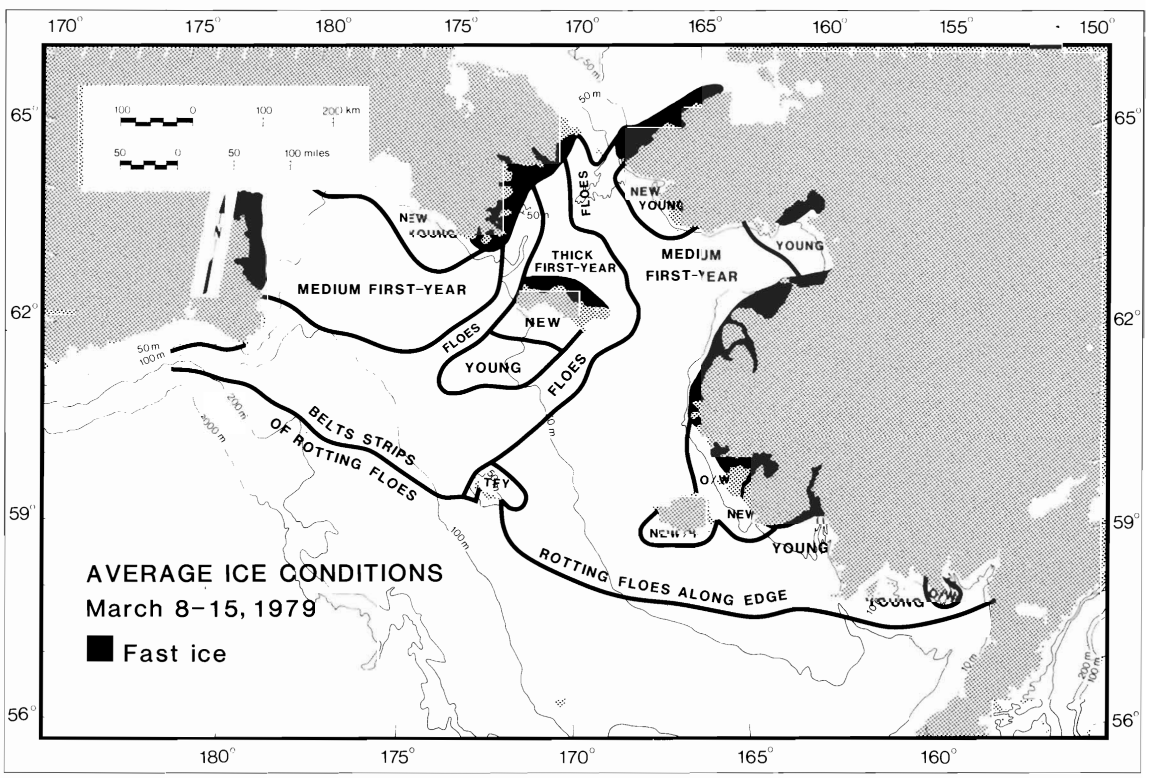

Figure 10-3. Weekly average ice conditions, 8-15 March 1979.

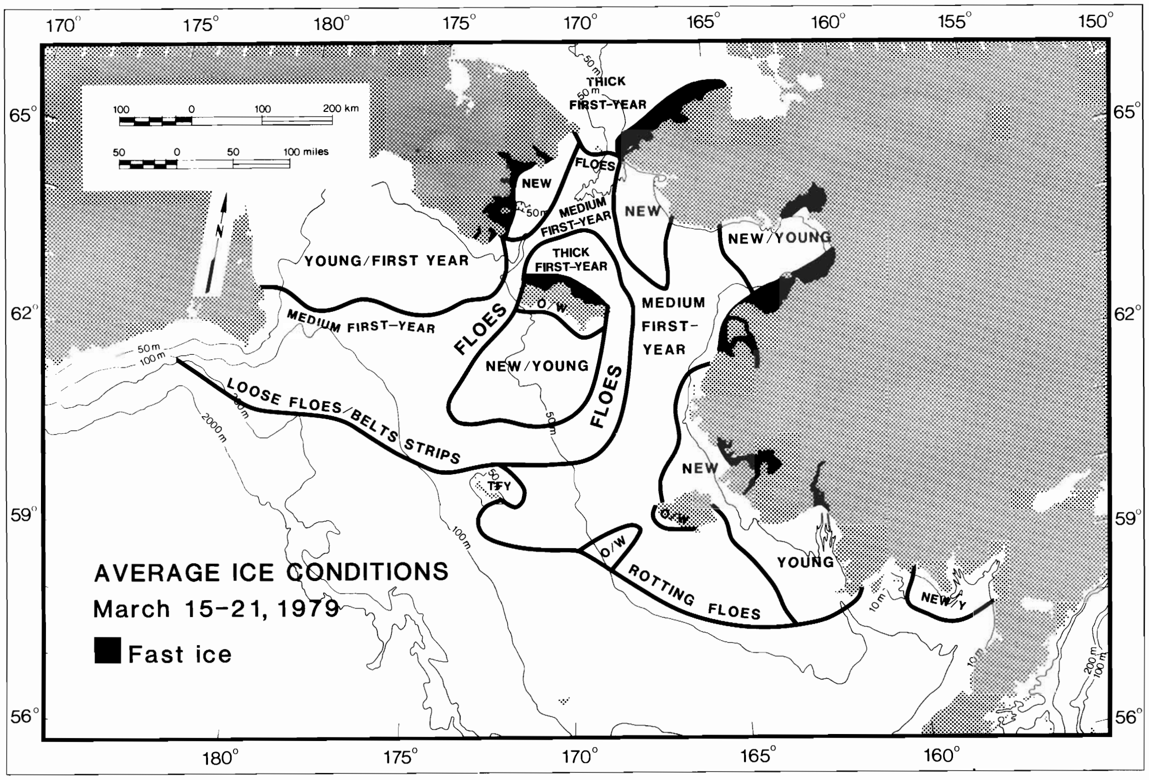

Figure 10-4. Weekly average ice conditions, 15-21 March 1979.

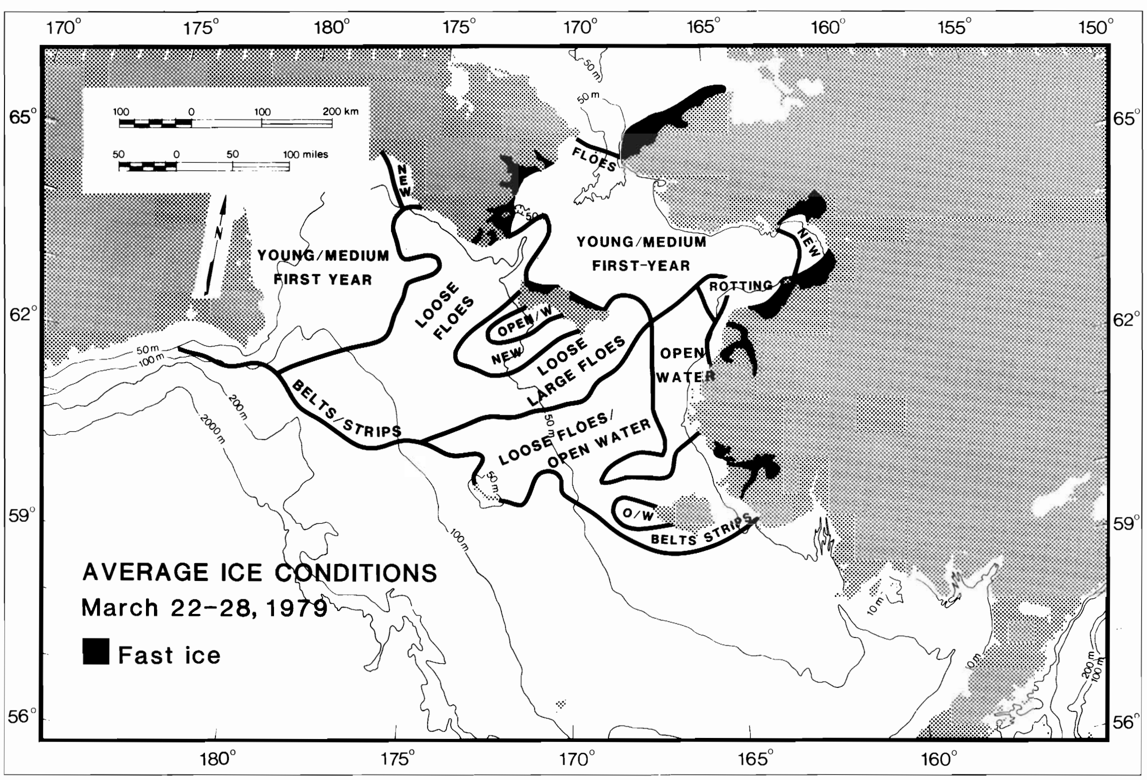

Figure 10-5. Weekly average ice conditions, 22-28 March 1979.

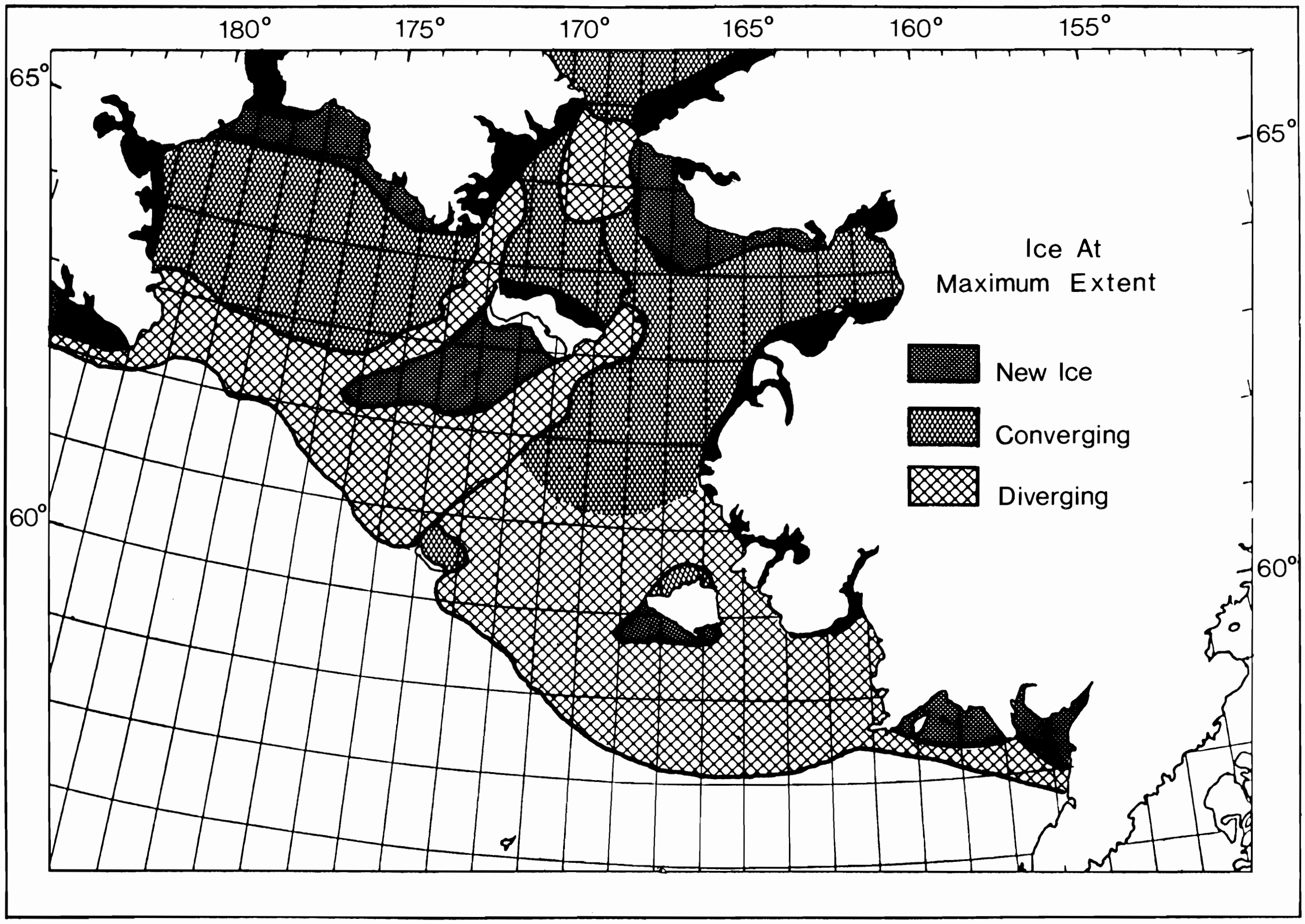

Figure 10-6. Schematic diagram of areas of ice generation, compaction, and divergence. This is meant as a first look for future refinement. The area of Eastern Norton Sound under certain wind conditions also behaves as an ice-formation area.

ICE FORMATION

In the initial stages of ice formation, grease ice is produced in the upper layer of the water and floats to the surface (Martin, Oil-Ice Interaction, this volume). This ice is blown downwind on the water's surface and piles up at the leading edge of ice streamers (Fig. 10-7). As the grease ice layer thickens, it damps the surface wave field (Martin, Oil-Ice Interaction, this volume) and is compacted until it forms a surface layer which can support ice growth underneath. This thickening ice forms pancakes and eventually larger floes which are incorporated into the pack. This replacement process appears to be continuous.

Fig. 10-8 shows a LANDSAT 3 image of the polynya area west of Nome along the Seward Peninsula. It has been enhanced to bring out detail in the first two gray levels of the image so that the grease ice forming in the lee of the mainland is visible. The wind was from the northeast (Pease, this volume). Streamers of grease ice can be seen, as well as large floes made of thin ice which was piled up and had broken free. Fig. 10-9, a mosaic of five LANDSAT 3 scenes from 12 March 1979, shows ice formation along a track from the Bering Strait to the ice edge near St. Matthew Island. Here grease ice is visible south of St. Lawrence Island. The gray signature of this thinner ice gradually appears whiter due to the thicker ice downwind. This polynya with grease ice forming within it was also noted during BESEX in 1973 (Ramseier et al. 1974), and is often evident in FWS ice charts (Eastern-Western Arctic Sea Ice Analyses, 1972-78). The wind was from the north (Pease, this volume).

Cores taken by Martin and Kauffman (1979) at the ice edge show that the upper portion of these floes consisted of a layer of consolidated grease ice. This was also observed in cores taken during BESEX in 1973 (Gloerson et al. 1974, Ramseier et al. 1974).

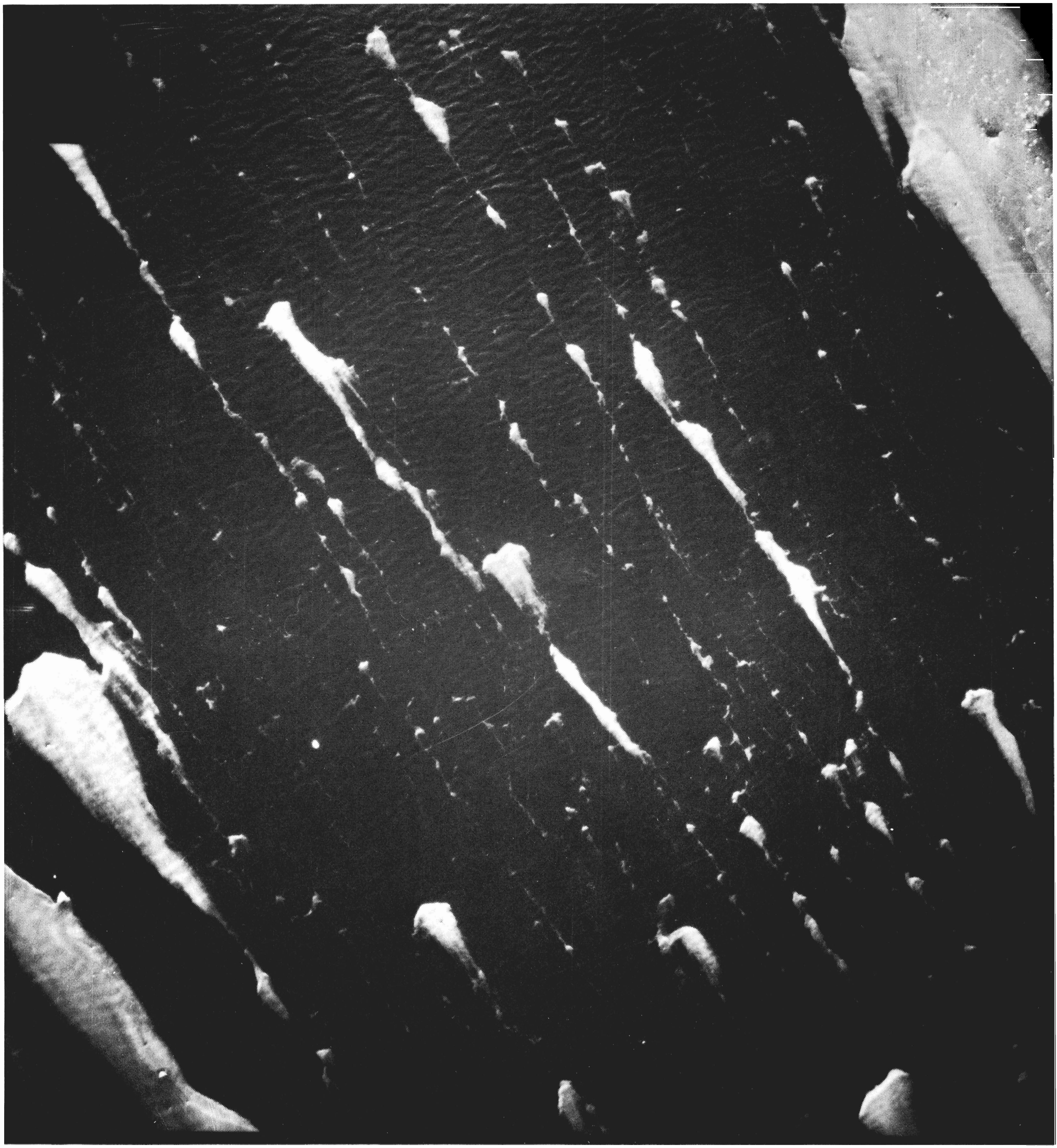

Figure 10-7. Grease ice photo taken from the CV990 aircraft during BESEX, 1973. (Courtesy of S. Martin, Univ. of Washington, NASA/Goddard). The ice is being blown downwind where it piles up at the leading edge. The grease ice streaks also damp the waves at the surface.

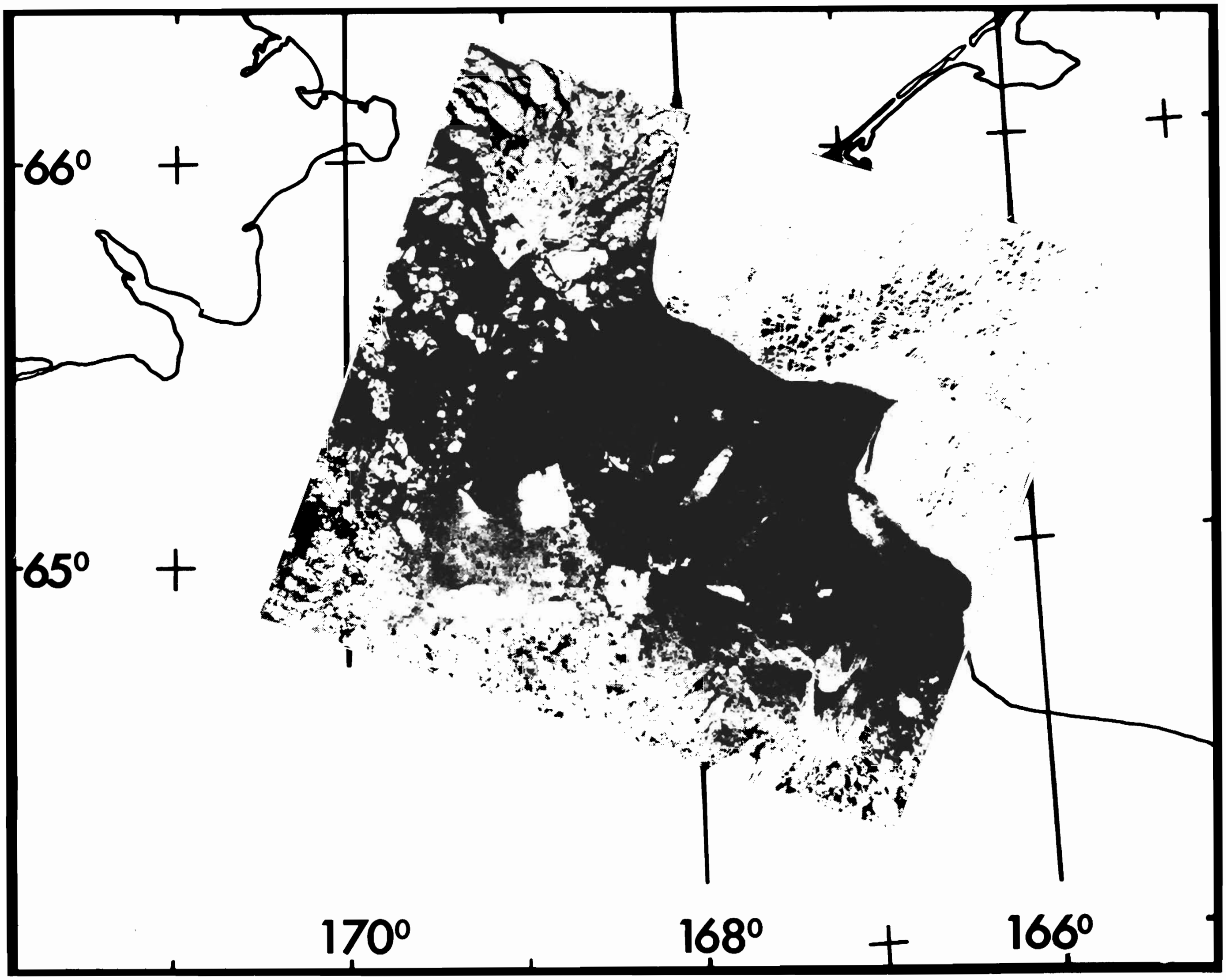

Figure 10-8. 2 March 1979, LANDSAT Imagery. This image has been enhanced to show details of the grease-ice formations in the leeward side of the shoreline.

These photographs support the hypothesis that the ice is formed to the north in large polynya areas and is blown south by the wind to the ice edge.

ICE COMPACTION

Ice in the Bering Sea, moving under the influence of the prevailing wind, tends to compact as it constricts or meets an obstacle. Sodhi (1977) and Shapiro and Burns (1975) show that this type of ice bridging often occurs north of St. Lawrence Island. FWS ice charts often show areas of thick first-year ice north of St. Lawrence, Nunivak, and St. Matthew islands (Eastern-Western Arctic Sea Ice Analyses 1972-78). Fig. 10-9 shows an example of such ice compaction. The wind is from the north and ice on the north side of St. Lawrence and St. Matthew Islands appears to be thicker, consistently white in appearance, and composed of tightly compacted floes with ridging structure evident on the surface. On the next day, 13 March, the LANDSAT 3 image (Fig. 10-10) shows that the same area of compaction north of St. Lawrence Island is relatively unchanged. The ice on both days was at maximum extent (Fig. 10-3).

The same phenomenon can be seen earlier in the month in the 2 March imagery from LANDSAT 3 (Fig. 10-11). The gray scale of the image differs significantly from the previous image because less light was available. However, the same areas of relative thickness can be seen north of St. Lawrence Island. The wind was from the northeast (Pease, this volume).

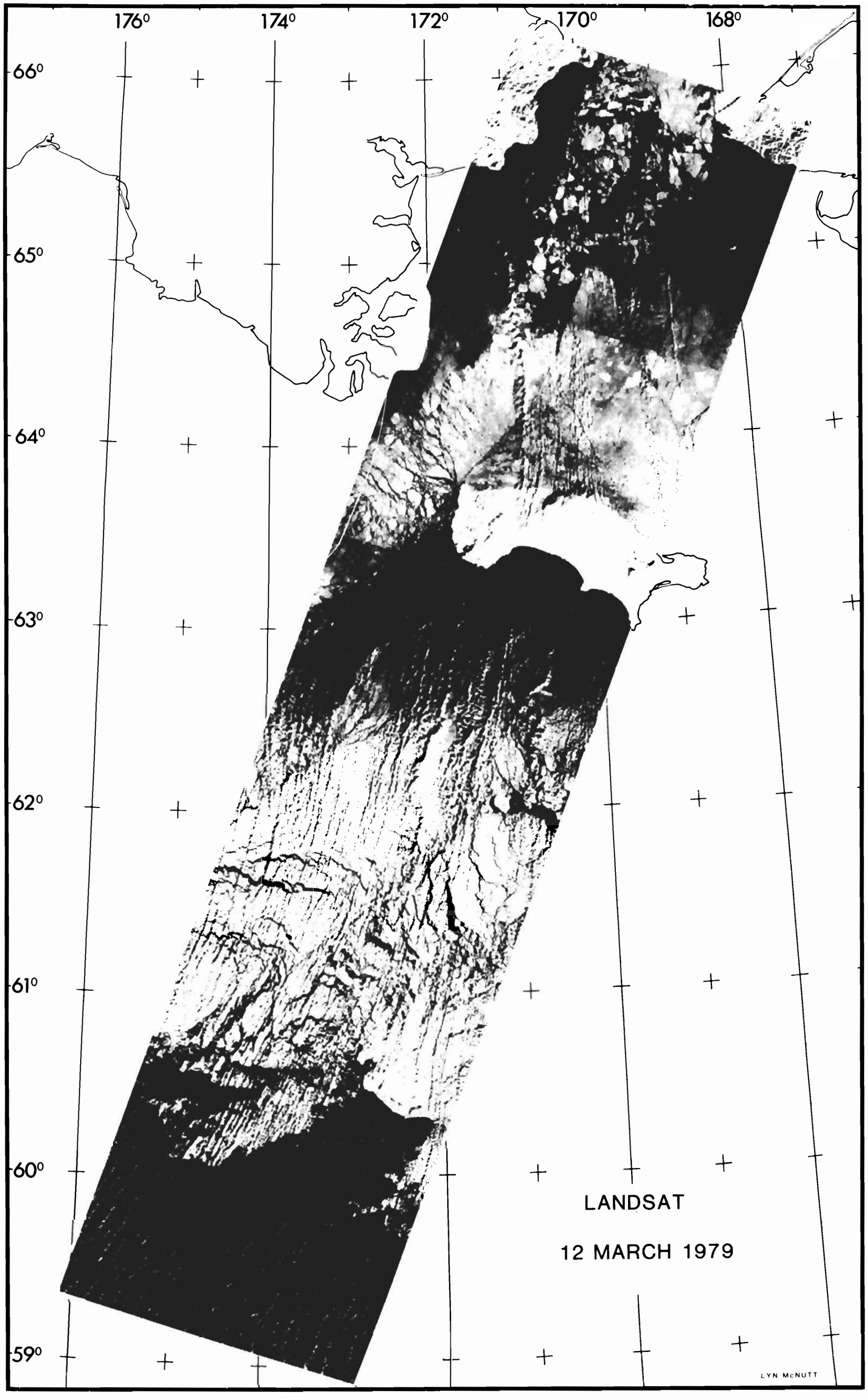

Figure 10-9. 12 March 1979, LANDSAT. This image is a mosaic of five separate scenes. It shows convergence north of St. Lawrence Island, St. Matthew Island, the polynya behind Lawrence Island, breakout of floes through Bering Strait, floes moving around St. Lawrence Island, ice streamers and bands at the edge, and roll cloud formation.

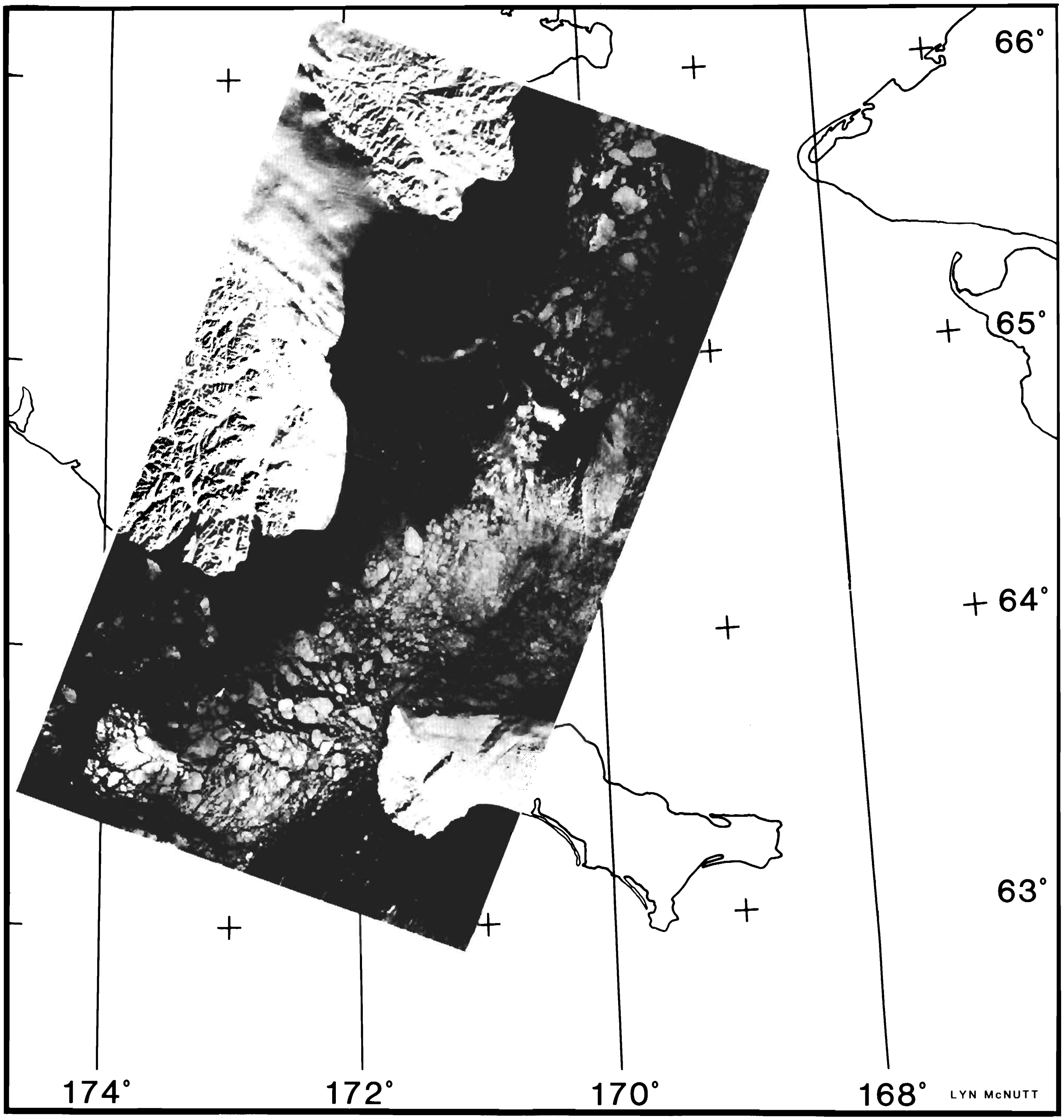

Figure 10-10. 13 March 1979, LANDSAT.

ICE DIVERGENCE

Ice which is compacting tends to raft and ridge until shearing causes portions of the ice to break off. The freed ice then separates from these bridging areas, causing leads to be formed (Sodhi 1977). This ice moves downwind as giant floes and vast floes in a matrix of smaller floes and brash ice (an accumulation of floating ice made of fragments <2 m across). This accounts for the areas with large floe streams in Figs. 10-1-10-5. This phenomenon shows up well in both Fig. 10-9 and 10-10, and was noted during the BESEX experiment by Ramseier et al. (1974), Gloerson et al. (1974), and Campbell et al. (1974). When locations of the leads and floes for both days are compared, it is seen that the floes have moved, and that the orientation of the leads remained consistent, approximately perpendicular to the wind.

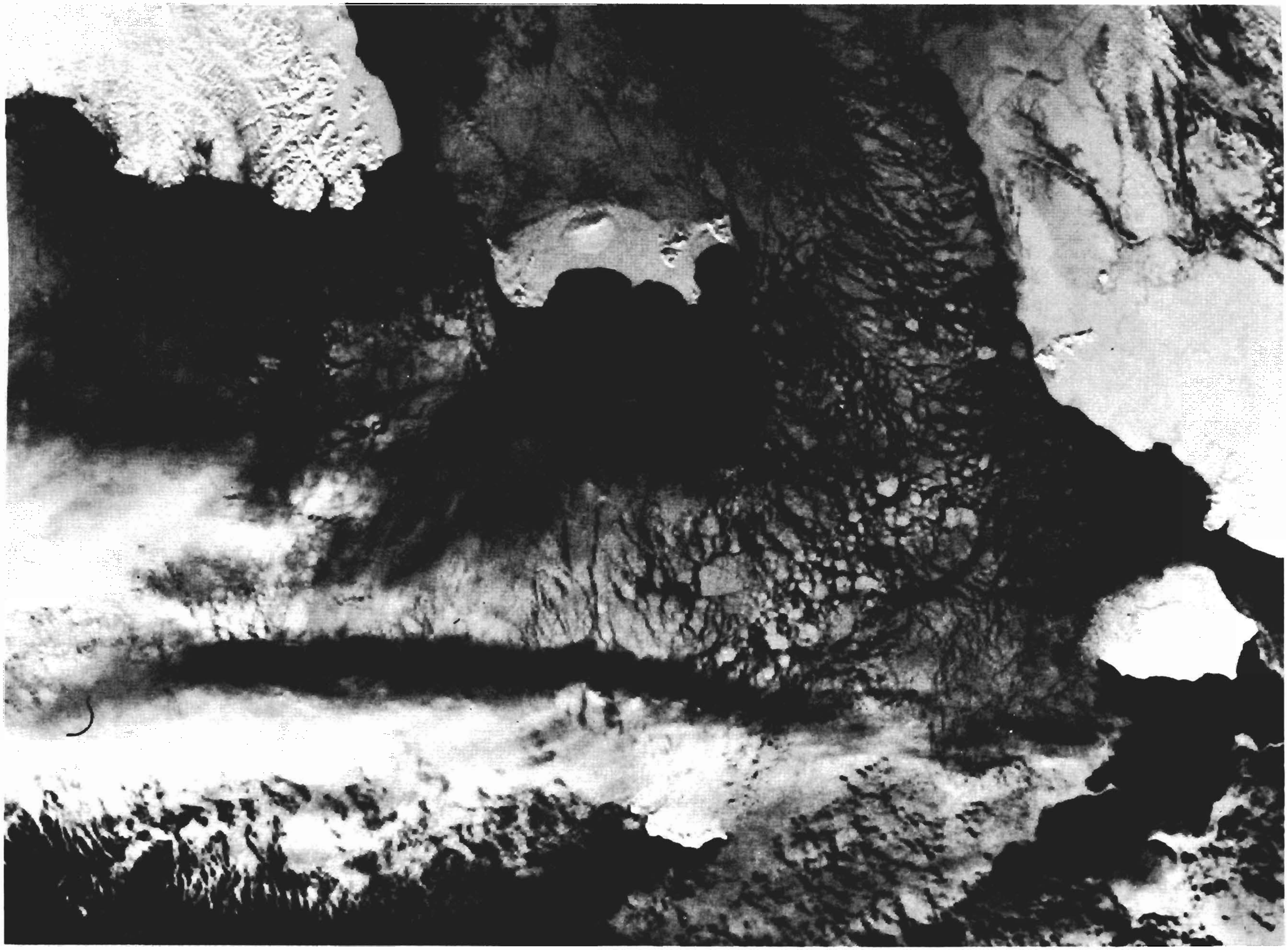

Figure 10-11. 16 March 1979, TIROS. This is an enlargement of a portion of the TIROS scene. Enlargements like this were used to track floes for 16, 17, 18, and 19 March.

A more detailed study of this phenomenon was undertaken using enhanced TIROS imagery for March 16, 17, 18, and 19 (Fig. 10-12), so that individual floes could be tracked for a longer period of time. Muench and Ahlnäs (1976) tracked floes during spring 1974 and found that their dominant direction of travel, in the area south of St. Lawrence Island, was to the south-southwest under predominantly northeast winds. Twelve floes A-G, J-N (Fig. 10-12), were tracked during the period 16-19 March for two days, and where possible for three days. Due to the resolution of the imagery, all floes appeared to be giant (>10 km across). Floes could not be tracked longer than three days because they tended to break up into floes smaller than the resolution of the imagery. Table 10-1 lists these floes by letter, gives their approximate size, the direction of the wind from true north (Pease, this volume), the floe direction, and the floe speed.

Floes A-G were followed on 16-17 March. For B-F the wind direction was estimated at 220°-225° relative to true north. The floes traveled 235° to 245°. For A and G the winds were estimated to be at 205° and the floes traveled 180°. These floes are within an area where their movement is affected by the ice shear around St. Lawrence Island. For floes

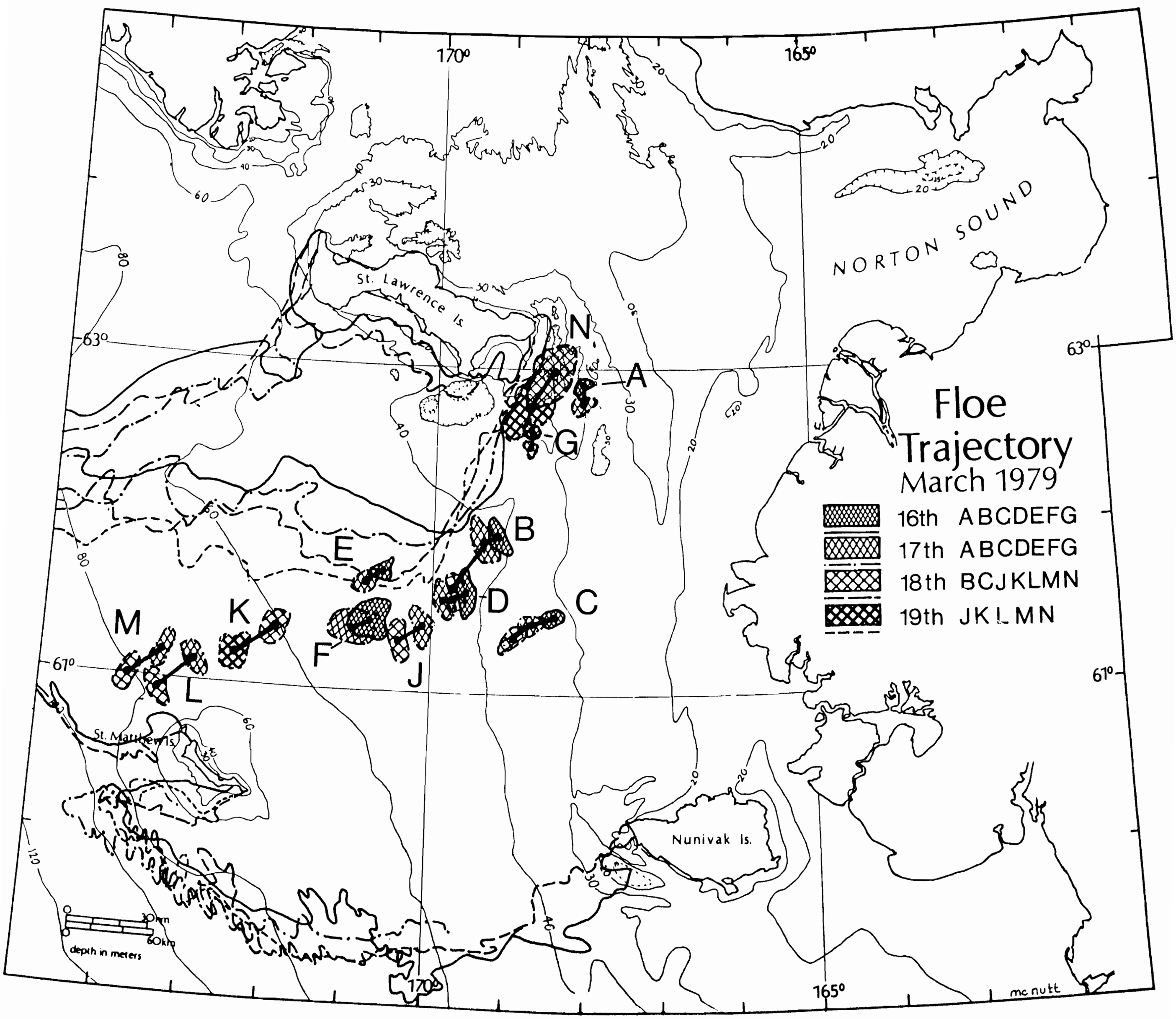

Figure 10-12. Floe trajectory map. 16-19 March 1979. The dominant wind regime was from the northeast during this period; floes tended to move to the south-southwest in response to the wind around the polynya area behind St. Lawrence Island.

TABLE 10-1

Floe trajectories, March 16 - 19, 1979

Floe	Wind direction (from true north)	Floe direction (from true north)	Floe velocity (m/sec)	Floe size (km)
A	205°	180°	.28	8X20
B	220°-230°	256°	.13	16X40
	220°-230°	218°	.50	16X40
C	220°-225°	252°	.23	12X20
	220°-225°	238°	.23	12X20
D	220°-225°	254°	.23	16X20
E	220°-225°	237°	.22	20X20
F	220°-225°	245°	.22	36X32
G	205°	180°	.22	12X12
J	230°-235°	238°	.28	16X36
K	230°-235°	238°	.46	30X28
L	230°-235°	230°	.41	16X32
M	230°-235°	235°	.39	14X34
N	210°	217°	.42	32X60

J-M, on the 18th and 19th, the winds were from 230° to 235° and the floes traveled 230°-238°. For N, the floe traveled 217° under winds estimated to be at 210°. All floe movements show a strong correlation with wind direction and appear to move to the south-southwest under the northeast wind regime which is dominant at that time of year (OCSEAP 1977). The ice movement is slightly to the right of the wind. This agrees with data reported by Sverdrup (1928). Floes B and C were tracked for three days and maintained the strong relationship between wind direction and direction of floe movement.

The average distance traveled by the floes during a 24-hour period was 26 km with a range of speed from 0.13 m/sec to 0.50 m/sec. The average speed was 0.26 m/sec. The velocity, distance, and direction of travel of these floes imply a strong divergence of ice within the pack downwind toward the ice edge. The lead orientation for the same period (Fig. 10-13) reflects the movement of the ice to the southwest under this wind pattern and suggests a movement of the ice toward the edge to the west of St. Matthew Island. SLAR data from the NASA C131 aircraft (Fig. 10-14) also show this lead pattern east of St. Lawrence Island in an area of large floes. Winds this day were also from the northeast (Pease, this volume).

ICE-EDGE PHENOMENA

Figs. 10-2 and 10-3 show little change in the location of the edge itself, yet floe studies indicate that volumes of ice from within the pack are being blown to the edge. In order to study the nature of the ice at the edge, ground truth data needed to be collected.

The NOAA ship *Surveyor* was stationed at the ice edge from 2 to 14 March 1979 (Pease 1979; Pease, this volume). On 14 March, two NASA aircraft flew over the ship while ground truth data were being collected. The flightline for the C131 is shown in Fig. 10-14. Fig. 10-15 shows the flight track from the C130 aircraft. An analysis of *in-situ* data on ice cores (Martin and Kauffman 1979) and floe drift, along with information on wave attenuation, shows that ice along the edge consists of rotten floes which have reached a thermodynamic limit of stability and have begun to melt (Martin and Bauer, Pease, this volume). A plot of the location of the isotherms of the water surface as observed during the cruise period shows that the −1 C isotherm moved southward with respect to the ice edge (Pease, this volume). The CTD casts taken also show a lens of less saline water extending out from the edge—evidence of melting (Pease, this volume).

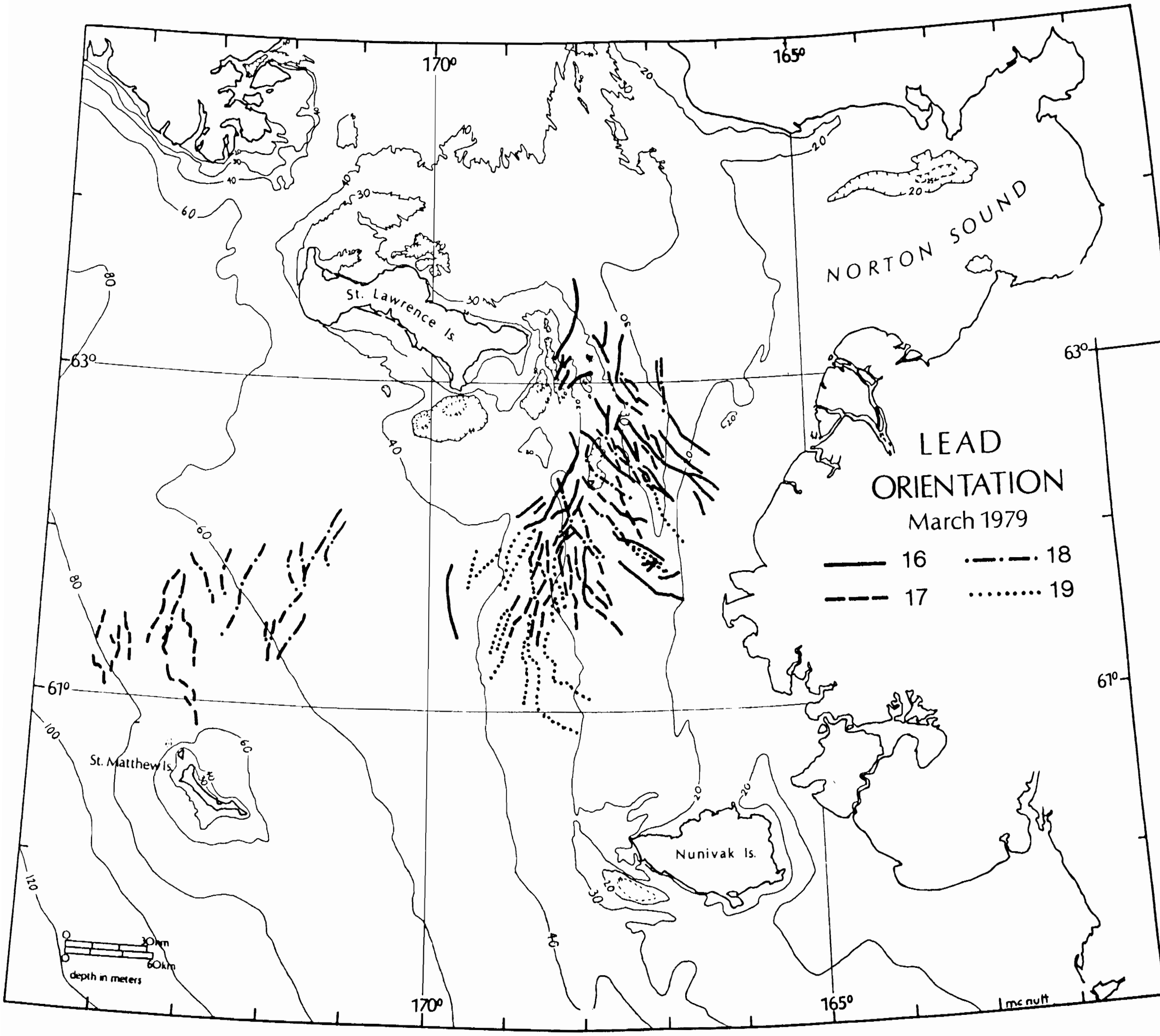

Figure 10-13. Lead orientation, 16-19 March 1979. Leads follow the same general trend downwind as the floes.

Satellite imagery such as that seen in Fig. 10-11, TIROS, and Figs. 10-9 and 10-10, LANDSAT, were used to study small-scale variations of these ice bands. These band features are not an isolated occurrence. They are often noted on FWS charts and have been studied by Muench and Charnell (1977). They can also be seen in a LANDSAT 3 image taken 5 March 1979 (Fig. 10-16), and on the 14 March imagery (Fig. 10-14).

An assessment of change in an ice band can be made using a photograph from the C130 overflight (Fig. 10-17). Although this image was taken approximately three hours earlier than the C131 SLAR image, the basic shape of the formation is still recognizable and can be seen to be made up of small, angular floes.

Similar photography from successive altitudes was used to study the characteristics of the floes within these bands. Fig. 10-18 shows a cross section of one of these bands. The distance across the band is 20 km. Darker floes in the middle of the band indicate thinner ice. The darker color and the nature of the surface patterns suggest that these floes are rotting. Ship's personnel who had occupied stations on similar floes reported that this type of ice was melting rapidly, and that it was thin enough to respond plastically to waves which were propagating through the ice (Pease 1979; Martin and Bauer, this volume).

Fig. 10-19, taken from a lower altitude, shows another cross section of a band. The flightline was from west to east, the wind from the northeast.

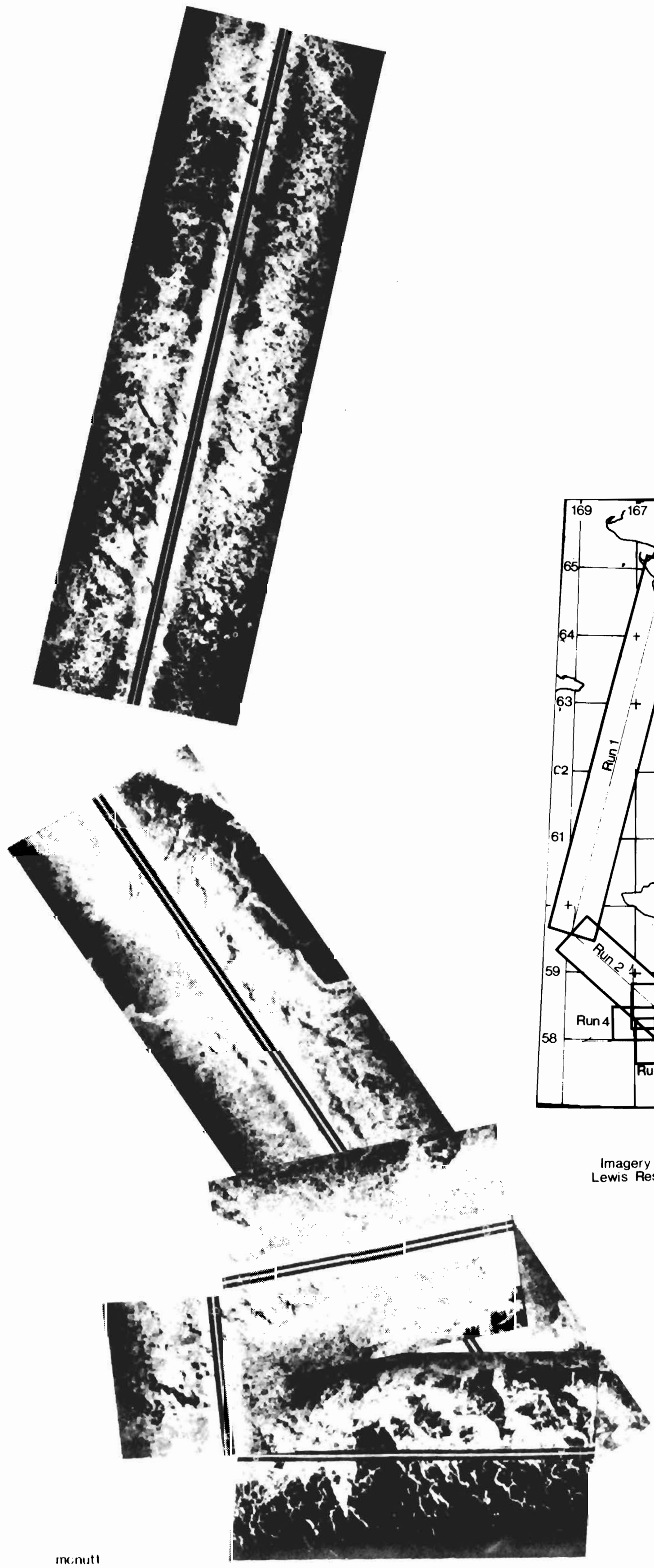

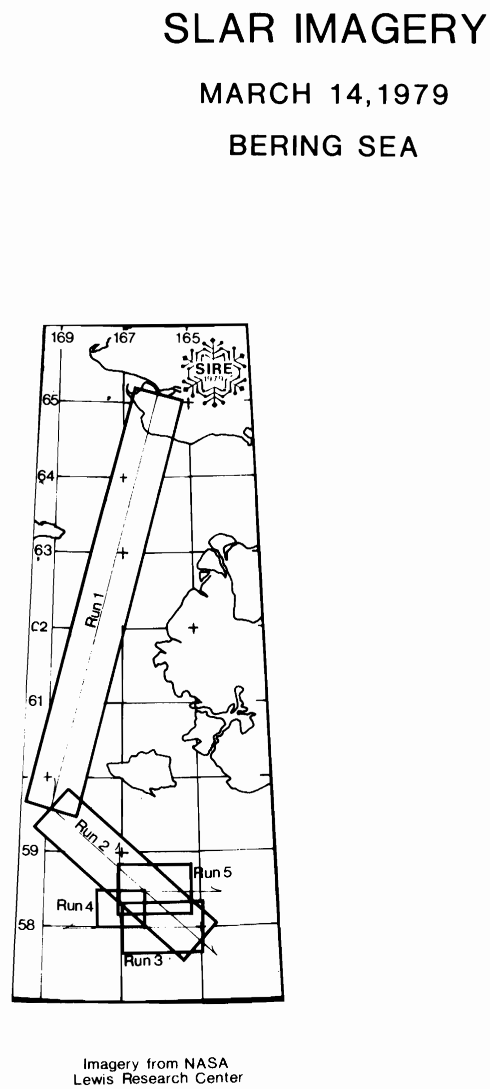

Figure 10-14. 14 March 1979, SLAR Mosaic. (Courtesy of R. Schertler, NASA/Lewis.) The C131 flightline is on the map at the middle right. Only the ice-edge lines and a portion of the long line from Nome are reproduced.

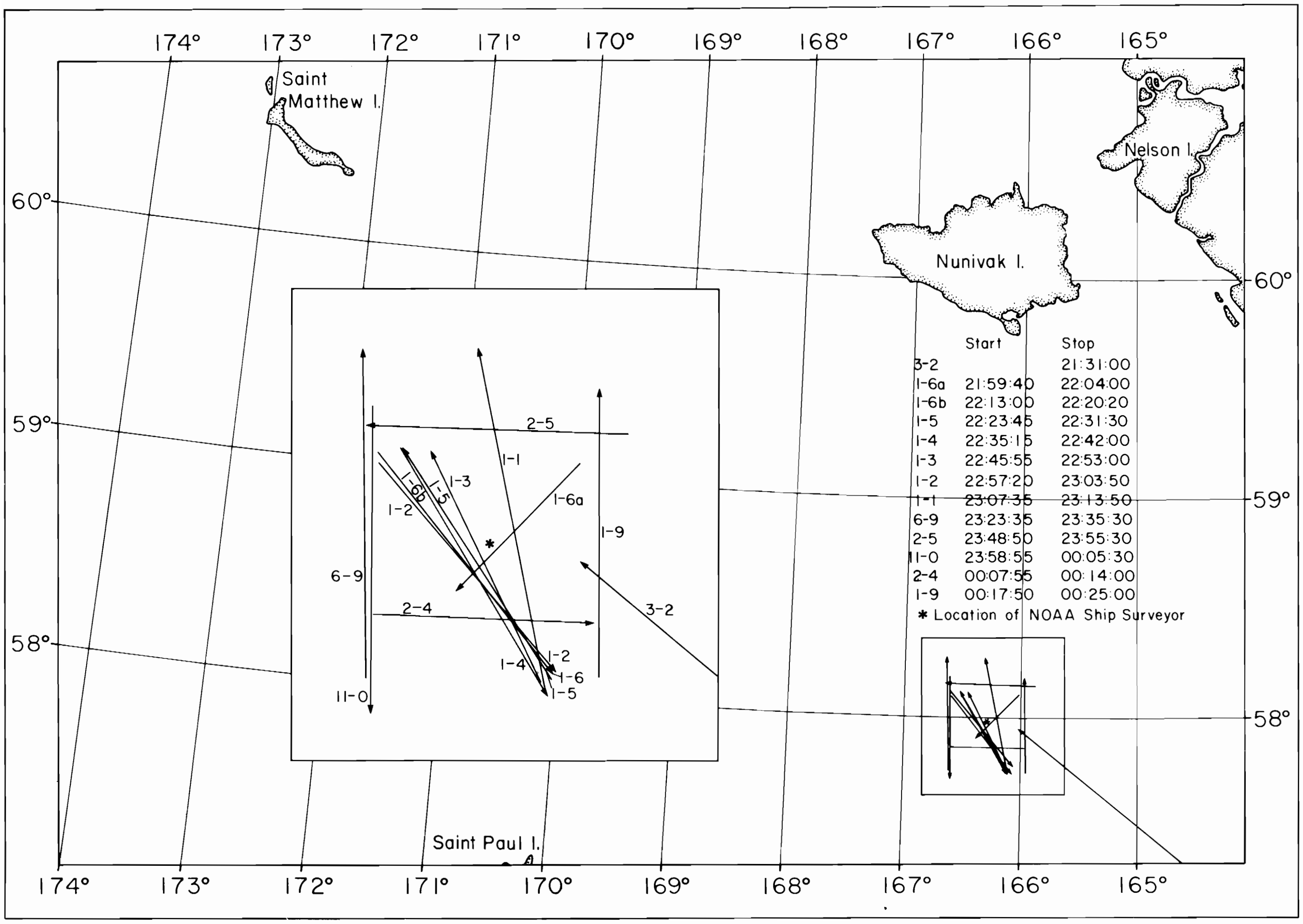

Figure 10-15. 14 March 1979, C130 flightline.

Smaller floes were blown downwind to the ice band. The leading edge of the band is made up of angular, thicker white ice floes. These floes are held together at the leading edge by the effects of the incoming swell; yet, as a group, they tend to move downwind at speeds of 0.3 m/sec (Martin and Bauer, this volume).

Fig. 10-20 shows the surface configuration of melting found on one of the thinner floes. This melting is not like that of Arctic ice, where melt puddles form on the surface of thick floes, but appears to be due to floe motions causing water to spill over the sides, and to the effects of a surrounding area of warmer water which causes the floe to rot. The two basic types of floes found at the edge were the highly rafted, relatively thick, white, angular floes (Fig. 10-21), whose freeboard allowed them to travel rapidly under the influence of the wind; and the thinner, larger floes (Fig. 10-22) found in the interior of the bands. These larger floes were variable in size, but were generally an order of magnitude larger than the white floes, which typically measured between 30 and 60 m in diameter. These sizes compare well with those measured by Martin and Kauffman (1979).

Martin and Bauer (this volume) have hypothesized that floes along the ice edge are formed from pack ice which is broken up at the edge by the effects of wind and incoming swell. First, the sheet ice is broken into vast rectangular floes whose width is proportional to the wavelength of the incoming swell (for an illustration, see Fig. 12-14, Martin and Bauer, this volume). These floes are further broken down and the thicker ice is rafted while being broken into small floes, which have sharp, angular edges, unlike pancake ice, which tends to be rounded. Pease (1979, this volume) noted from CTD casts along the ice edge that there is a surface lens of less saline, warmer water extending from the ice edge—evidence of meltwater. Preliminary returns analysed from the step-frequency radiometer on board the C130 tend to support

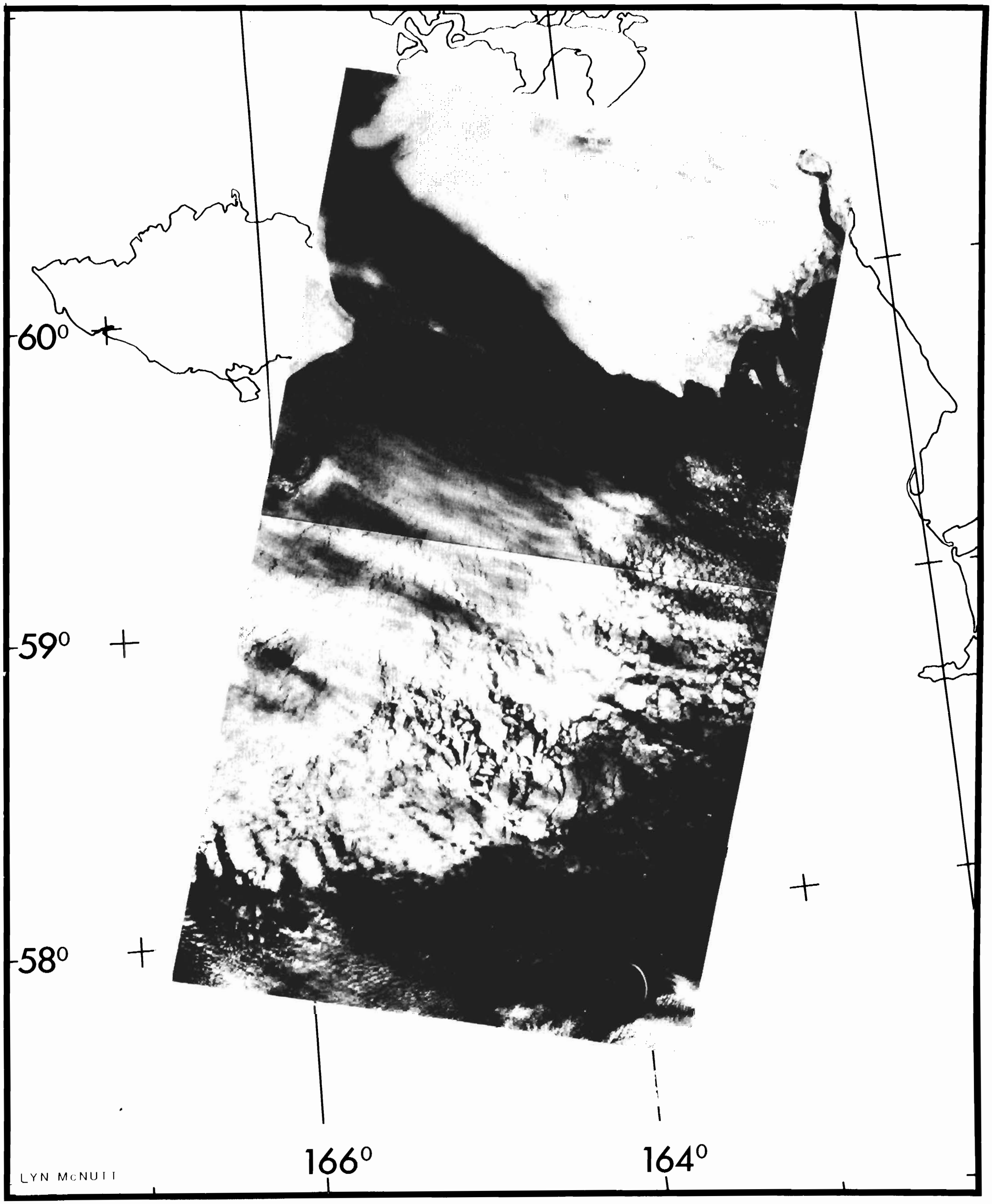

Figure 10-16. 5 March 1979, LANDSAT. This is a two-image mosaic showing ice bands to the southeast of Nunivak Island.

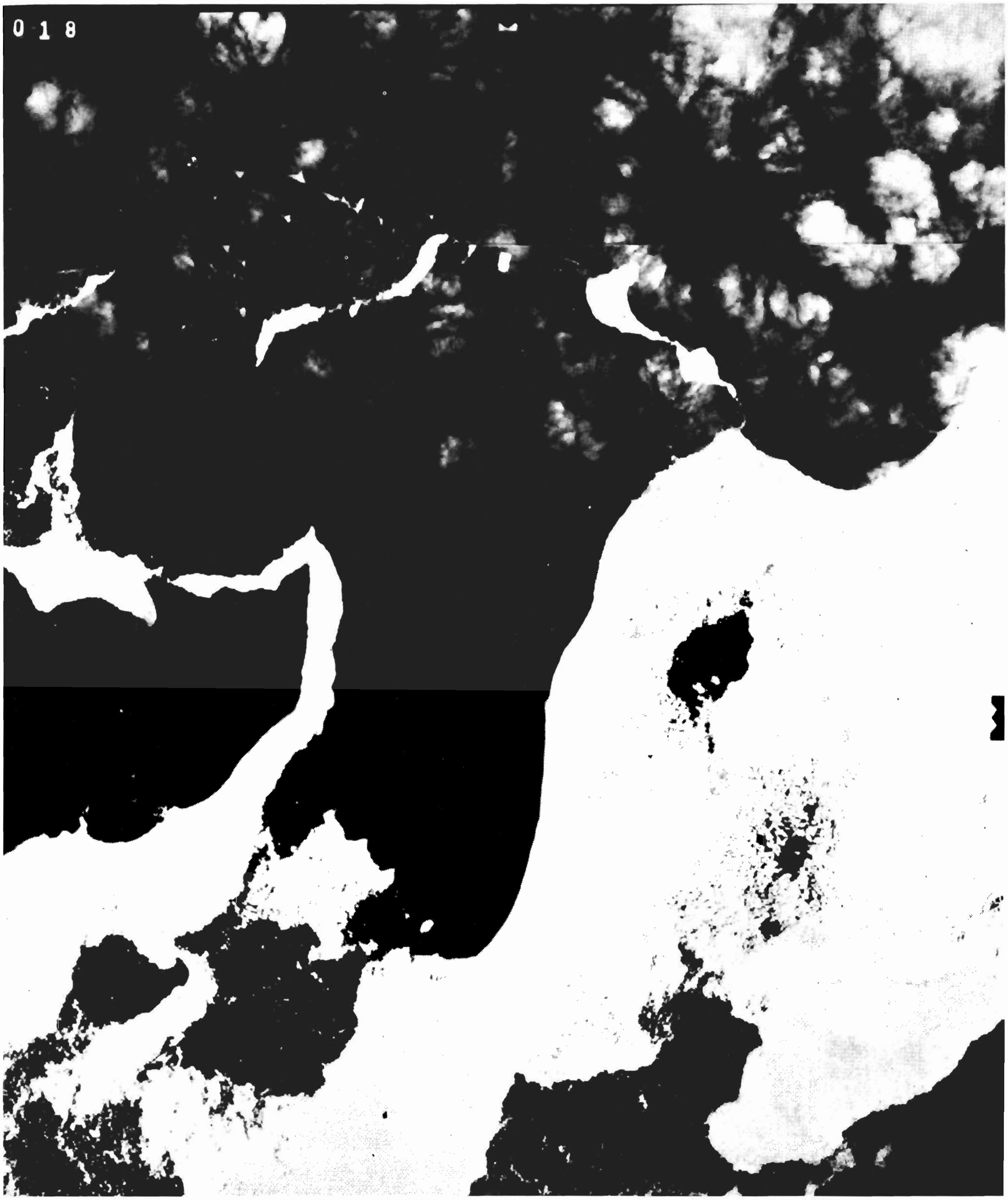

Figure 10-17. 14 March 1979, C130 photo mosaic of an ice band also seen in the 14 March SLAR data run.

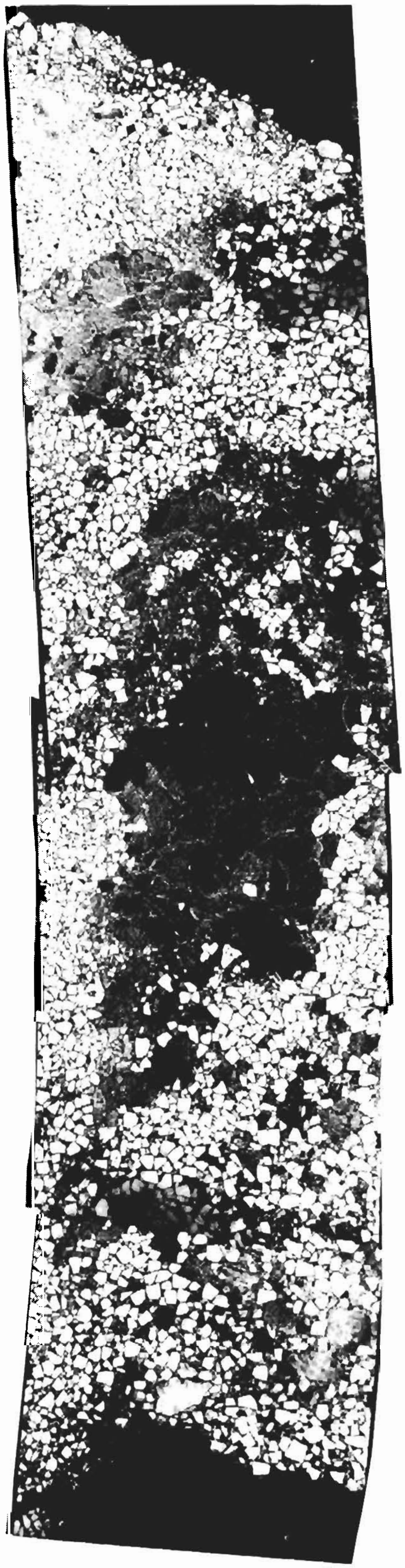

Figure 10-18. Ice band near the NOAA ship *Surveyor*, showing the two types of ice in a band approximately 20 km across. The light-colored, angular floes are thicker ice; the darker ice near the center is thinner, melting ice.

Figure 10-19. Ice band near the NOAA ship *Surveyor*. The flightline was from west to east (left to right), the wind was from the northeast. Ice fragments can be seen to be advecting downwind to the band. The leading edge of the band is loosely held together by the influence of incoming swell.

Figure 10-20. Two-frame mosaic of thinner ice near the interior of an ice band. The floes show the effects of melting along the edges and in the center, especially.

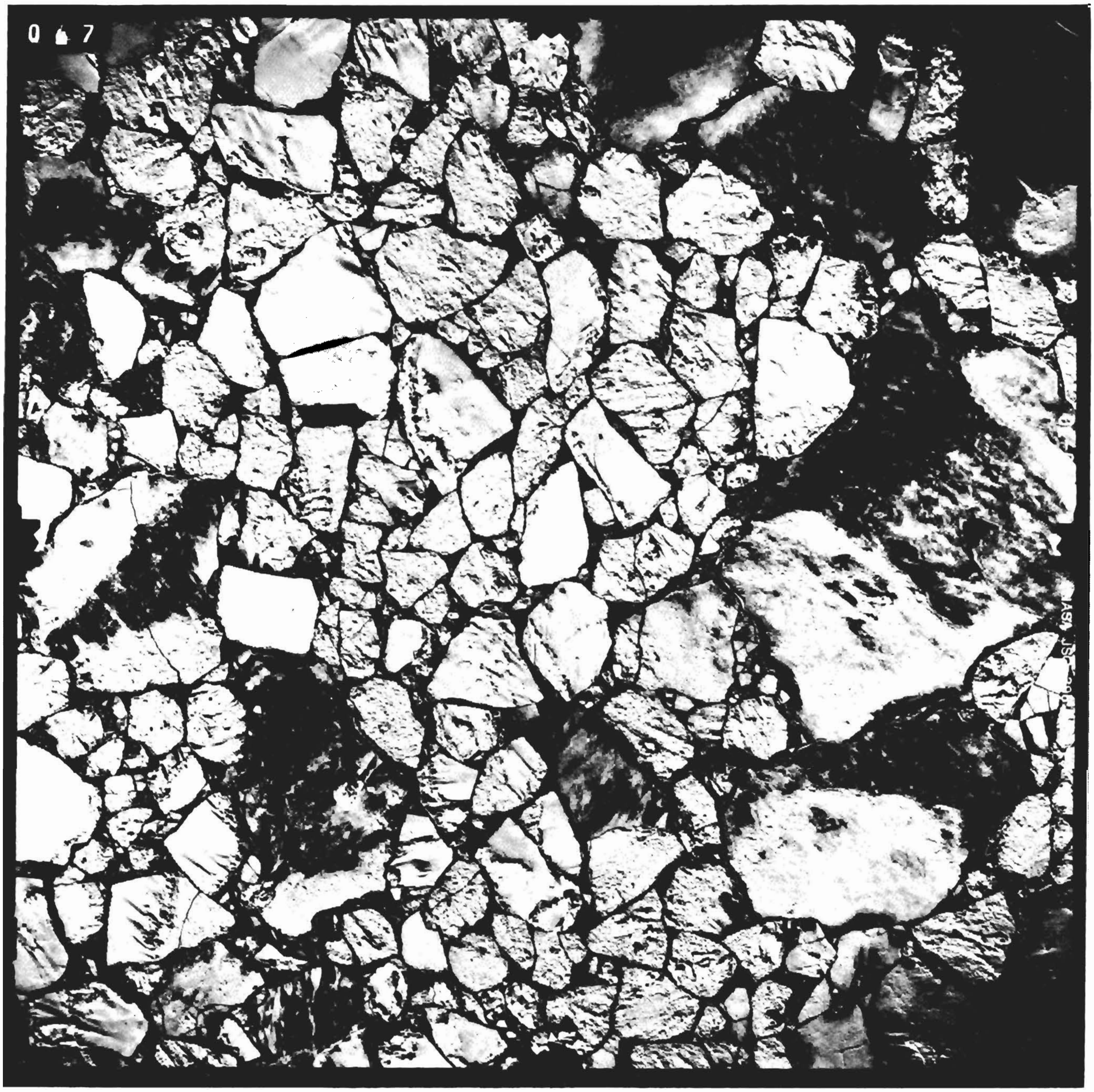

Figure 10-21. Detail of thicker, rafted white floes. Note the angular edges and the presence of snow on the surface. The floes are 30-60 m in size.

this hypothesis. The return from the radiometer indicates that the ice is relatively fresh and occurs as a matrix of less-saline water than would normally be found on the surface (Swift, personal communication).

ICE RETREAT

At the end of March 1979, the ice in the Bering Sea began a rapid retreat. This can be seen rather dramatically by comparing the 16 March TIROS

Figure 10-22. Detail of thin, melting floes. Note the lack of snow on the surface and thaw holes.

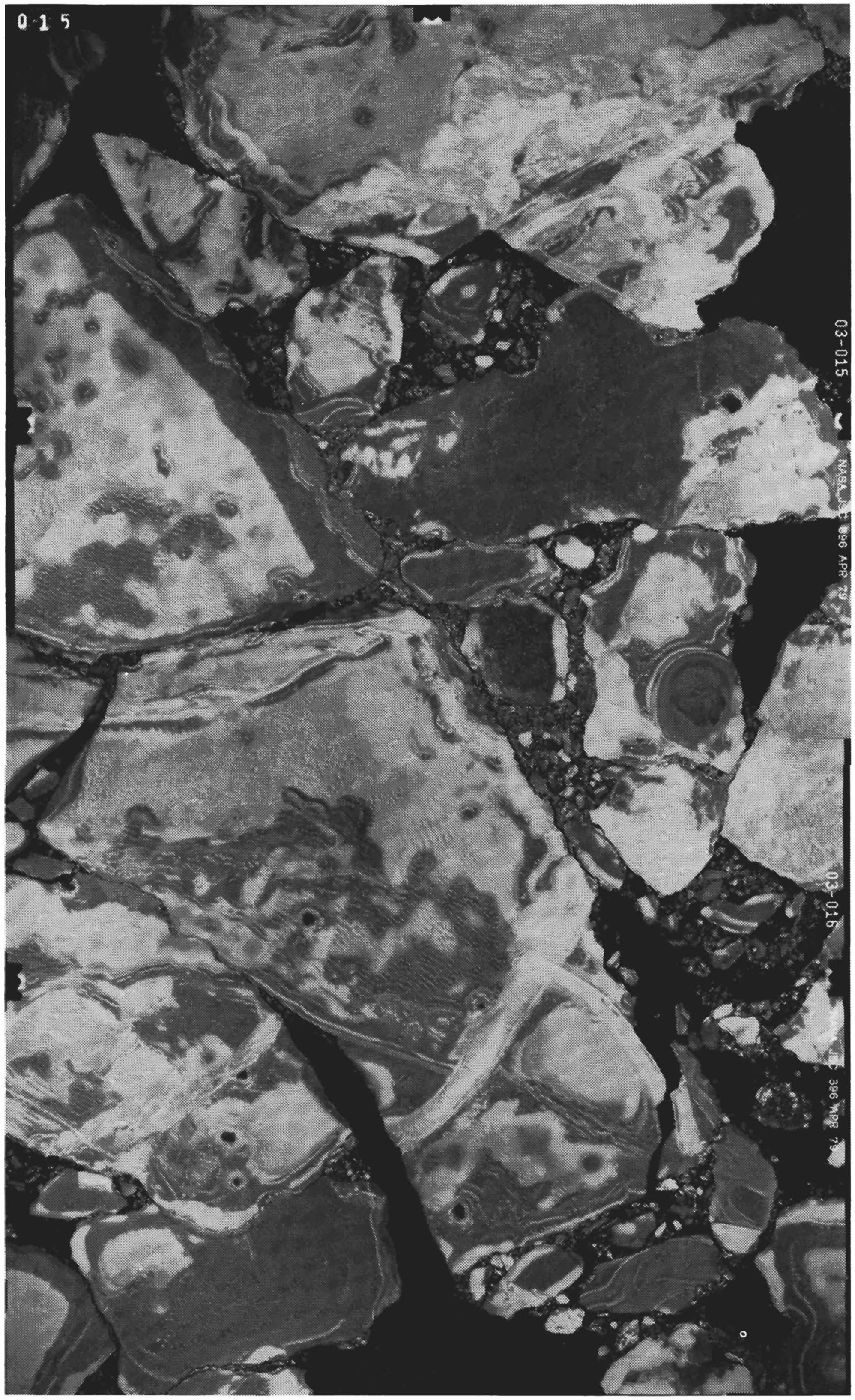

image (Fig. 10-11) with the 26 March TIROS image (Fig. 10-23). This period of retreat coincided with a time of maximum insolation and warm southerly winds generated by a low over the Aleutians (Pease, this volume). A comparison of Fig. 10-23 with the average weekly chart for 22-28 March (Fig. 10-5) shows the meltback proceeding in the eastern Bering Sea between the coast and Nunivak and St. Lawrence Islands, an area into which ice is continually advected (Fig. 10-6). It is interesting to note the persistence of the floes around St. Lawrence Island. The SLAR data for March 27 (Fig. 10-24) shows an open water/thin ice area north of St. Lawrence Island (McNutt 1977), more leads present on the eastern edge of St. Lawrence Island, and open areas and new leads in Norton Sound.

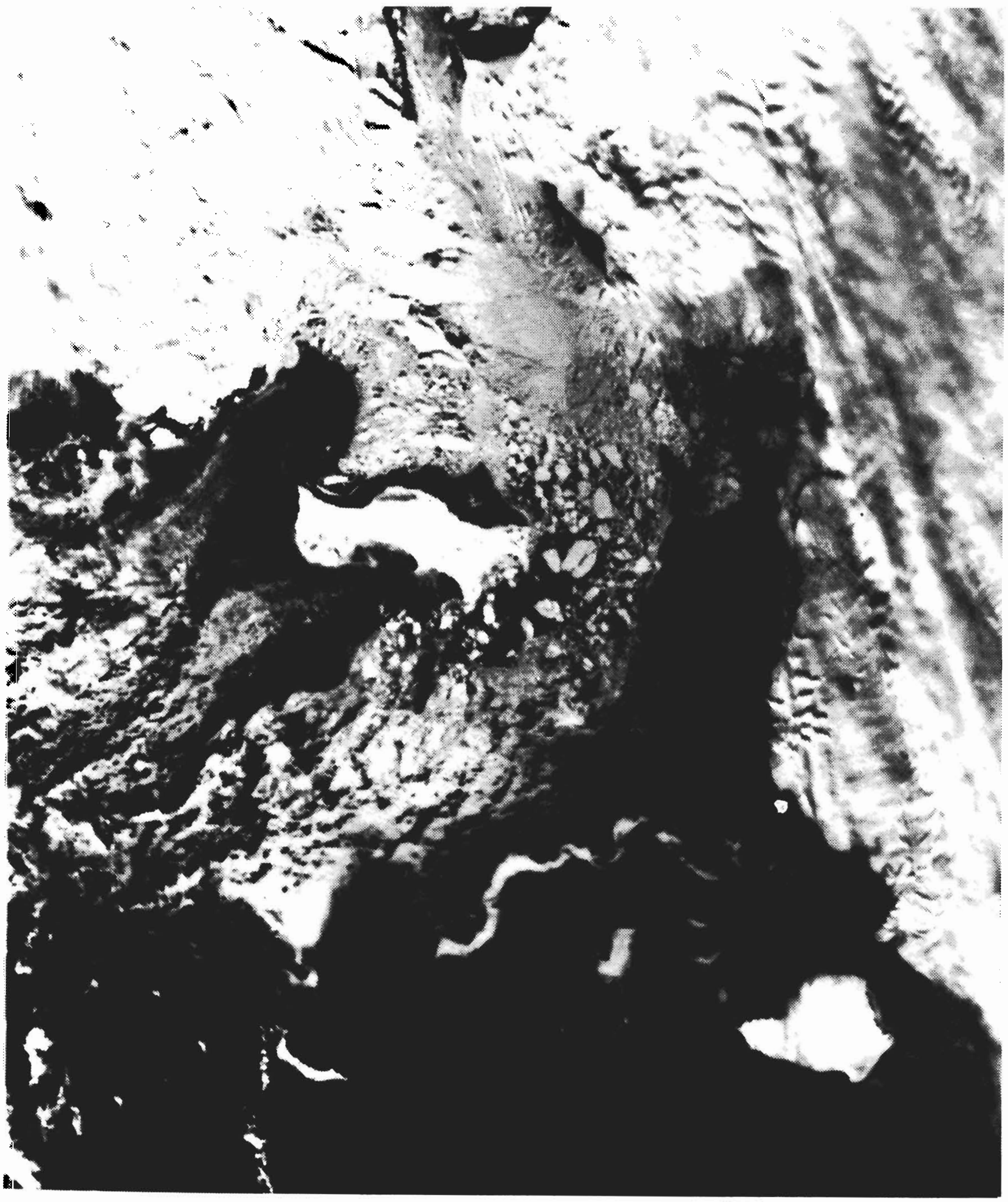

Figure 10-23. 26 March 1979. This TIROS enlargement shows the effects of a rapid meltback. (Compare with Fig. 10-11.)

SLAR IMAGERY

MARCH 27,1979

NORTON SOUND

Imagery from NASA Lewis Research Center

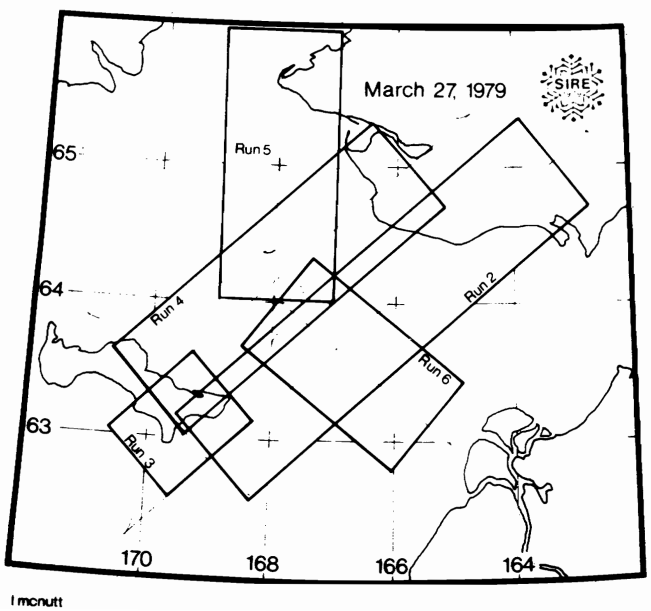

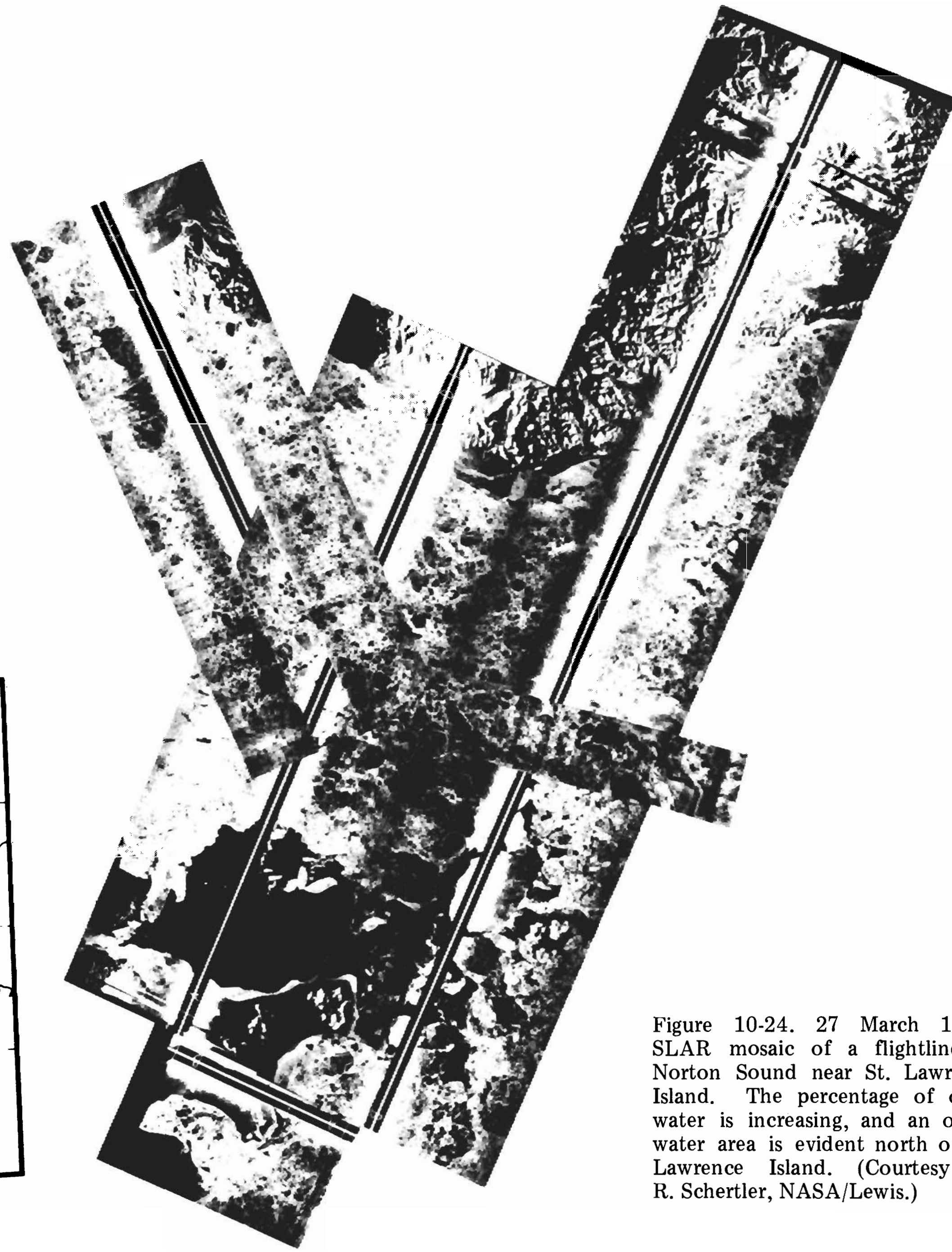

Figure 10-24. 27 March 1979. SLAR mosaic of a flightline in Norton Sound near St. Lawrence Island. The percentage of open water is increasing, and an open-water area is evident north of St. Lawrence Island. (Courtesy of R. Schertler, NASA/Lewis.)

The ice during this period of meltback appeared to be retreating most rapidly in areas which had previously been supplied by ice blown down from the north. The change of wind direction from north-northeast to south-southeast affects floe trajectories and tends to blow ice to the north instead of to the south-southwest. One would not expect to find ice bands along the edge under these conditions, and yet isolated, string-like features of ice persist in areas which are otherwise ice free (Fig. 10-23). In some areas, e.g., the area to the southwest of St. Lawrence Island, ice persists and remains relatively motionless. More work needs to be done to study the effects of wind, insolation, and water temperature on ice movement during this retreat.

CONCLUSIONS

The 1978-79 ice season was a relatively light ice year, perhaps because of short-term climatic variations in the mean annual sea surface temperatures (Niebauer, this volume). March 1979 was unique, in that one month encompassed conditions of maximum extent and rapid retreat. When the Bering Sea ice is at maximum extent, it reaches a steady state in which ice is formed in polynyas on the leeward side of east-west trending coasts and advected downwind. The ice bridges along the northern coasts of islands and shear zones existing on both sides of the wedge of thicker ice. Floes are broken off at these shear zones and, under north-northeast wind conditions, floes originating on the eastern side of St. Lawrence Island drift south-southwest towards the ice edge near St. Matthew Island. Ice at the edge is broken up by the effects of wind and incoming swell and is blown downwind into ice bands. Ice in these bands reaches its thermodynamic limit and melts along the edge. During the breakup the ice retreats under the effects of increased insolation and southerly winds. The ice near the coast, which had been diverging from the north, is no longer replenished and retreats first. Under continued southerly wind conditions, individual floes may begin to migrate northward.

ACKNOWLEDGMENTS

This work is Contribution No. 443 from the NOAA Pacific Marine Environmental Laboratory. Writing of the manuscript was funded, in part, by NOAA/NESS/SPOC Group Project #MO-A01-78-00-4335. Reproduction of the satellite imagery would not have been possible without the skills of Jim Anderson, PMEL.

REFERENCES

Ahlnäs, K., and G. Wendler
1979 Sea observations in the Bering, Chukchi and Beaufort Sea, Proceedings of POAC—79, Norwegian Inst. Tech.

Campbell, W. J., P. Gloerson, and R. O. Ramseier
1974 Synoptic ice dynamics and atmospheric circulation during the Bering Sea experiment. Results of the US contribution to the joint US/USSR Bering Sea experiment. NASA/Goddard (NASA X-910-74-141).

Fleet Weather Facility
1975 Western Arctic sea ice analysis, 1972-1975. Capt. S. L. Balmforth, C. O. Suitland, Maryland.

1976 Eastern-western Arctic sea ice analysis. Cmdr. V. W. Roper, C. O. Suitland, Maryland.

1977 Eastern-western Arctic sea ice analysis. Capt. J. A. Jepson, C. O. Suitland, Maryland.

1978 Eastern-western Arctic sea ice analysis. Cmdr. J. C. Langemo, C. O. Suitland, Maryland.

Gloerson, P., R. Ramseier, W. J. Campbell, T. C. Chang, and T. T. Wilheit
1974 Variation of the morphology of selected microscale test areas during the Bering Sea experiment. Results of the U.S. contribution to the joint U.S./U.S.S.R. Bering Sea experiment. NASA/ Goddard (NASA X-910-74-141).

Harrington, R. F.
1979 An airborne remote sensing 4.5 to 7.2 Gigahertz stepped frequency microwave radiometer. Proc. IEEE Microwave Symposium.

Loshchilov, V. S.
1974 Characteristics of the ice cover in the operational area of the "Bering" expedition (1973), Preliminary results of the Bering expedition, 18-30.

Martin, S., and P. Kauffman
1979 Data report on the ice cores taken during the March 1979 Bering Sea ice edge field cruise on the NOAA ship *Surveyor*, Univ. of Washington, Dep. of Oceanogr., Spec. Rep. No. 89.

McNutt, S. L.
1977 Interpretation key for microwave discrimination of sea ice characteristics, M.A. Thesis, UCLA.

Muench, R. D., and K. Ahlnäs
1976 Ice movement and distribution in the Sea from March to June, 1974, J. Geophys. Res. 81(24).

Muench, R. D., and R. L. Charnell
1977 Observations of medium-scale features along the seasonal ice edge in the Bering Sea, J. Phys. Oceanog. 7(4).

OCSEAP
1977 Climate atlas of the outer continental shelf waters and coastal regions of Alaska, 2, Bering Sea. Arctic Environmental Information and Data Center, Anchorage, Alaska.

Pease, C.
1979 Cruise report for NOAA ship *Surveyor* 28 Feb. - 17 March, 1979, NOAA, PMEL, Seattle, Wash.

Ramseier, R. O., P. Gloerson, W. J. Campbell, and T. C. Chang
1974 Mesoscale description for the principal Bering Sea ice experiment. Results of the U.S. contribution to the joint U.S./U.S.S.R. Bering Sea experiment. NASA Goddard (NASA X-910-79-141).

Schertler, R.
1979 Background information on copy negatives of LeRC original SLAR/ Imagery, Lewis Research Center/ NASA.

Shapiro, L. H., and J. J. Burns
1975 Satellite observation of sea ice movement in the Bering Strait region. Climate of the Arctic, Rep. Univ. of Alaska, Fairbanks.

Sverdrup, H. V.
1928 The wind-drift of the ice. *In:* The Norwegian polar expedition with the *Maud* 1918-1925, Scientific results, IV: 1. A. S. John Griegs Boktrykkeri, Bergen.

Sodhi, D. S.
1977 Ice arching and drift of pack ice through restricted channels. U.S. Corps of Eng., CRREL Rep. 77-18.